PROCEEDINGS, 51st Workshop on Geothermal Reservoir Engineering
Stanford University, Stanford, California, February 9-11, 2026
SGP-TR-230

Thermal Decline and Management in Energy Generation from Fractures in Super Hot Rock Formations

Sharat Chandrasekhar, P.V. Suryanarayana

Blade Energy Partners, 2800 Network Blvd, Ste 550, Frisco, TX 75214 USA

schandrasekhar@blade-energy.com

Keywords: Energy Extraction, Super-Hot Rock Formations, CLGS

ABSTRACT

Geothermal wells drilled into super-hot rock formations have the potential to generate significant levels of thermal power in closed loop geothermal systems. In addition, a properly designed system of wells can meet target electric power demands even after accounting for conversion losses. The most efficient means of working fluid enthalpy gain is through a network of fractures connecting a pair of injector (cold fluid) and riser (hot fluid) wells, thereby maximising fluid-to-formation contact area. The motivation behind many projects is usually based on the rough estimates of thermal power due to the difference between the well inlet and undisturbed geothermal temperatures. This ignores however the fact that in the vicinity of the fractures, the geothermal temperature declines with time. In addition, the problem is exacerbated when the cold fronts from adjacent fractures coalesce. Larger spacing between fractures to mitigate this effect comes at the expense of fewer fractures in the available space.

This study investigates both decline mechanisms and design optimisation strategies to combat them in the aforementioned scenarios. Since the thermal transients cannot be correctly estimated with a pseudo-transient approach, a fully transient model taking into account heat transfer in both the fracture and formation is necessary. Semi-analytical solutions of the energy equation are developed, and it is shown how thermal decline can be managed with a mass flow rate schedule. The results indicate that fracture geometry and resource temperature are by far the most significant contributors to efficient energy generation. Larger spacing between fractures helps arrest thermal decline, but this effect tends to diminish once the spacing is substantially greater than the thermal front progression, or if high mass flow rates cause early coalescing of the cold fronts from adjacent fractures. It is hoped that the results from this study will prove useful in the design of many enhanced and closed loop geothermal systems.

1. INTRODUCTION

In response to the near-universal consensus that renewable forms of energy are essential to meeting global energy demand, geothermal energy is emerging as an attractive option owing to its ability to generate a sustained baseload for several years. Conventional geothermal energy generation requires access to a hydrothermal source, and while attractive from a high baseload capacity standpoint, is limited in geographical extent. In this context, there has been a renewed interest in Advanced Geothermal Systems (or AGS), and classical Enhanced Geothermal Systems (EGS), which have the potential to extract heat from hot dry rock. All of these systems involve the creation of an engineered heat exchange system within the resource. Many variants of these systems have been proposed, most of which essentially connect two (or more) wells through the engineered heat exchanger in the resource.

The earliest demonstration of the concept appears to be the Fenton Hill study (see, for example, Brown, et al., 2012). Since then, advances in EGS have greatly enhanced its commercial viability as evidenced by the recent projects of Fervo (Norbeck et al, 2023) and Utah FORGE (Allis and Moore, 2019). Both these demonstration projects were at temperatures around 200 °C. More recent advances include connecting multilaterals between injector and riser wells in Super Hot Rock (SHR) formations (with resource temperatures greater than 375°C), as in the study by (Holmes, et al., 2021). Moncarz and Suryanarayana, 2022 presented an approach involving thermal reach enhancement which featured the novel concept of the insertion of high conductivity materials in the formation to enhance heat transfer. A comparative study of several closed loop geothermal systems (CLGS) can be found in Beckers, et al., 2022). The potential of using EGS in SHR formations evinced the interest of the US Department of Energy, 2024 which issued several grants to companies to explore the concept further. And in 2025, Mazama Energy demonstrated EGS at a record high average resource temperature of 331 °C[1].

In a couple of recent studies (Chandrasekhar et al. (2024), Suryanarayana and Chandrasekhar, 2025) we introduced a scaling parameter that governs heat transfer from the formation to the working fluid in geothermal wells. This parameter (which we christened the Γ parameter) is analogous to the Number of Transfer Units concept in heat exchanger analysis, which is consistent with the fact that a geothermal well is an engineered heat exchanger through which circulation of a working fluid (typically water, although Supercritical CO_2 has been proposed as an alternative) extracts heat from the resource and generates power through a surface power cycle. With time however, a cold front propagates out into the formation due to the colder fluid being injected into the resource. This phenomenon is referred to as *thermal decline*, and successful base load power generation must take this into consideration. The study of Suryanarayana and Chandrasekhar (2025) addressed thermal decline in the concept of instantaneous maximum power and not base load generation. That

[1] Trent Jacobs, "Mazama Energy Reports Record 629°F Enhanced Geothermal System at Oregon Volcano", *JPT*, Nov 11, 2025

study used a pseudo-transient snapshot-in-time approach following Ramey (1962) and is not capable of correctly addressing continuous steady power generation.

In this study, we consider power generation from a pair of injector and riser well connected by several planar fractures. We perform a fully transient approach similar to that of Gringarten (1975), except that unlike the constant mass flow rate assumption in Gringarten's study, we consider sequential operations where the mass flow rate variation with time can be regulated to manage the power at a target value. The solution of the transient transport equation in the fracture is connected to the analytical solution of the transient diffusion equation in the formation through Duhamel Convolution Integrals embedded in a Fourier series. It is shown how the full thermal legacy of the system can be propagated through the Duhamel integrals. The effect of the spacing between fractures is also explored. Several illustrative examples are presented and a parametric sensitivity analysis of key parameters is performed.

2. PROBLEM DESCRIPTION

The idealisation of a network of fractures connecting two horizontal conduits is shown in Figure 1. Cold fluid from the surface entering a lateral conduit passes through the fractures where it picks up heat from the formation and returns through the other lateral conduit to the surface where it can be used to generate power or be a source of direct heat. The flow directions in the resource section shown are more conducive to a CLGS where the riser exit is in closer proximity to the injector inlet, than if the flow direction in the horizontal portion of the riser well were reversed.

The following assumptions are invoked in the thermal model:

1) The fractures are thin rectangular conduits all of which have the same length, breadth, and thickness, as indicated
2) The fractures are all spaced a uniform distance apart
3) The flow rate from the supply conduit is distributed evenly amongst the fractures.
4) Lateral variations of temperature (in the $x-$ and $y-$ directions are negligible
5) Constant thermophysical properties prevail throughout the conduits and in the formation.
6) the flow is fully developed only in a hydrodynamic, but not a thermal sense. Therefore the pressure and velocity transients are ignored.
7) The kinetic energy term is negligible compared to the thermal and pressure energy terms, and is therefore omitted from the energy transport equation.
8) Heat transfer in the formation is assumed to be solely conductive[2]. Further, heat diffusion in the formation is limited to the $x-$ coordinate direction. Accordingly, while the formation temperature varies in both the $x-$ and $z-$ coordinate directions, the second derivative in the latter direction is ignored in the energy equation.

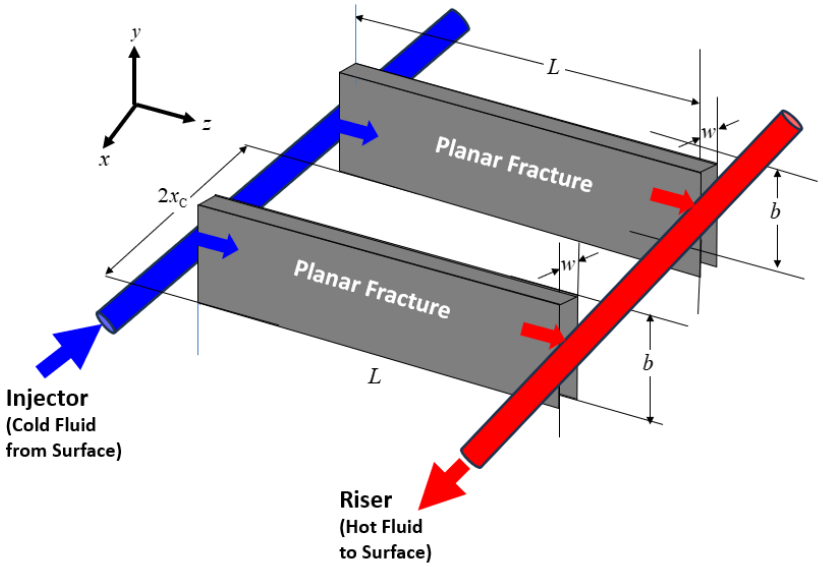

Figure 1. Flow across a network of Planar Fractures in a Hot Rock Formation.

[2] This is a conservative assumption and applicable to most dry rock resources. In some resources, the presence of water may provide convective support. Likewise, proximity to magma fingers, or presence of radioactive decay may provide a heat source that can support heat transfer. These effects are not considered in the work.

2.1 Governing Equations

With respect to the coordinate system in Figure 1 and the assumptions stated above, the transient energy equation in a single conduit can be written as

$$\rho_{\mathrm{f}} c_{\mathrm{p_f}} \frac{\partial T_{\mathrm{f}}}{\partial t} + \rho_{\mathrm{f}} c_{\mathrm{p_f}} V \frac{\partial T_{\mathrm{f}}}{\partial z} = 2 \frac{k_{\infty}}{w} \frac{\partial T_{\mathrm{g}}}{\partial x} \tag{1}$$

where T_{f} and T_{g} are the area-averaged temperatures and V is the bulk velocity in a single fracture defined as

$$V = \frac{\dot{m}}{\rho A_{\mathrm{f}}} = \frac{\dot{m}}{\rho b w} \tag{2}$$

Equation (1) is subject to the initial condition wherein the entire fracture is at the resource temperature, i.e.,

$$T_{\mathrm{f}}(z,0) = T_{\infty} \tag{3}$$

and the inlet boundary condition

$$T_{\mathrm{f}}(0,t) = T_{\mathrm{in}} \tag{4}$$

where T_{in} is the temperature entering the fractures from the injector well, Transient diffusion in the formation is described by the breadth-averaged equation

$$\rho_{\infty} c_{\mathrm{p}_{\infty}} \frac{\partial \overline{T}_{\mathrm{g}}}{\partial t} = k_{\infty} \frac{\partial^2 \overline{T}_{\mathrm{g}}}{\partial x^2} \tag{5}$$

subject to the initial condition

$$\overline{T}_{\mathrm{g}}(x,0) = \overline{T}_{\infty} \tag{6}$$

and the boundary condition at the fracture-formation interface

$$\overline{T}_{\mathrm{g}}(0,t) = \overline{T}_{\mathrm{f}}(t) \tag{7}$$

where the *a priori* unknown fracture temperature is to be determined in tandem with the solution of Eq. (1). The distant boundary condition is a vanishing flux owing to symmetry at the mid plane between two fractures, i.e.,

$$\frac{\partial \overline{T}_{\mathrm{g}}}{\partial x}(x_{\mathrm{C}},t) = 0 \tag{8}$$

2.2 Nondimensionalisation

It is convenient to cast the governing equations in non-dimensional form prior to establishing solutions. Therefore a set of dimensionless variables is introduced

$$\xi = \frac{z}{L} \qquad \eta = \frac{x}{w} \qquad W = \frac{x_{\mathrm{C}}}{L} \qquad \tau = \frac{\alpha_{\infty}}{w^2} t \tag{9}$$

where the dimensionless time is effectively a Fourier Number, and the temperatures are normalised according to

$$\theta_{\mathrm{f}} = \frac{T_{\infty} - T_{\mathrm{f}}}{T_{\infty} - T_{\mathrm{in}}} \qquad \theta_{\mathrm{g}} = \frac{T_{\infty} - T_{\mathrm{g}}}{T_{\infty} - T_{\mathrm{in}}} \tag{10}$$

Substitution of Eqs. (9) and (10) into Eqs. (1)--(4) transforms the energy equation in the fracture to

$$\frac{\partial \theta_{\mathrm{f}}}{\partial \tau} + \Omega \frac{\partial \theta_{\mathrm{f}}}{\partial \xi} = \Psi \left. \frac{\partial \theta_{\mathrm{g}}}{\partial \eta} \right|_{\eta=0} \tag{11}$$

subject to the initial condition

$$\theta_{\mathrm{f}}(\xi,0) = 0 \tag{12}$$

and the inlet boundary condition

$$\theta_{\mathrm{f}}(0,\tau) = 1 \tag{13}$$

and in the formation, Eqs. (5)--(8) are transformed to

$$\frac{\partial \theta_{\mathrm{g}}}{\partial \tau} = \frac{\partial^2 \theta_{\mathrm{g}}}{\partial \eta^2} \tag{14}$$

subject to the initial condition

$$\theta_{\mathrm{g}}(\eta,0) = 0 \tag{15}$$

and the boundary conditions

$$\theta_{\mathrm{g}}(0,\tau)=\theta_{\mathrm{f}}(\tau) \tag{16}$$

and

$$\frac{\partial\theta_{\mathrm{g}}}{\partial\eta}(W,\tau)=0 \tag{17}$$

In Eq. (11) the dimensionless parameters are defined as

$$\Omega=\frac{1}{2}\frac{\alpha_{\mathrm{f}}}{\alpha_{\infty}}\frac{w}{L}\left(\frac{\dot{m}c_{\mathrm{p_f}}}{k_{\mathrm{f}}b}\right) \tag{18}$$

and

$$\Psi=2\frac{(\rho c)_{\infty}}{(\rho c)_{\mathrm{f}}} \tag{19}$$

2.3 Fracture-Formation Interface Flux

It is shown in Appendix A that the solution of the transient diffusion equation in the formation yields the interface flux as the Fourier series

$$\left.\frac{\partial\theta_{\mathrm{g}}}{\partial\eta}(\tau)\right|_{\eta=0}=-\frac{2}{W}\sum_{k=0}^{\infty}D_k(\tau) \tag{20}$$

where the Duhamel Convolution Integral is

$$D_k(\bar{\tau}_N)=e^{-\lambda_k^2\tilde{\tau}}D_k\left(\bar{\tau}^{(n-1)}\right)+\int_0^{\bar{\tau}_N-\bar{\tau}_{N-1}}e^{-\lambda_k^2(\tilde{\tau}-\beta)}\frac{\partial\phi_{\mathrm{f}}}{\partial\beta}\mathrm{d}\beta \tag{21}$$

with $D_k(0)=0$ for all Fourier modes and where he interval 0 to τ has been divided into several subintervals each with possibly different mass flowrates as indicated in Figure 2 such that the convolution integral in Eq. (A.6) can be split as in Eq. (21) which it should be noted is purely in terms of the local fluid temperature in the fracture. The objective is to be able to solve the energy equation within each of the temporal sub-intervals indicated in Figure 2, in conjunction with the interface flux that is continuously evolving from time zero, as represented by the Duhamel Integrals corresponding to each Fourier mode as given by Eq. (A.8). This is accomplished by introducing a local time variable

$$\tilde{\tau}=\tau-\bar{\tau}^{(n-1)} \tag{22}$$

and the translation

$$\phi_{\mathrm{f}}(\xi,\tilde{\tau})=\theta_{\mathrm{f}}(\xi,\tilde{\tau}+\bar{\tau}^{(n-1)}) \tag{23}$$

whereupon substitution of Eq. (A.8) into Eq. (A.5) and subsequently into the energy equation of Eq. (11) yields in terms of the local time variable and translated temperature $\phi_{\mathrm{f}}(\xi,\tilde{\tau})$

$$\frac{\partial\phi_{\mathrm{f}}}{\partial\tilde{\tau}}+\Omega^{(n)}\frac{\partial\phi_{\mathrm{f}}}{\partial\xi}=-2\frac{\Psi}{W}\sum_{k=0}^{\infty}\left[e^{-\lambda_k^2\tilde{\tau}}D_k\left(\bar{\tau}^{(n-1)}\right)+\int_0^{\tilde{\tau}}e^{-\lambda_k^2(\tilde{\tau}-\beta)}\frac{\partial\phi_{\mathrm{f}}}{\partial\beta}\mathrm{d}\beta\right],\quad 0\le\tilde{\tau}\le\bar{\tau}^{n}-\bar{\tau}^{(n-1)} \tag{24}$$

subject to the local initial condition

$$\phi_{\mathrm{f}}(\xi,0)=\theta_{\mathrm{f}}(\xi,\bar{\tau}^{(n-1)}) \tag{25}$$

and the time-invariant boundary condition

$$\phi_{\mathrm{f}}(0,\tilde{\tau})=1 \tag{26}$$

The solution of the Integro-Differential Equation above using Laplace Transformation in conjunction with the Convolution Theorem is also explained in Appendix A.

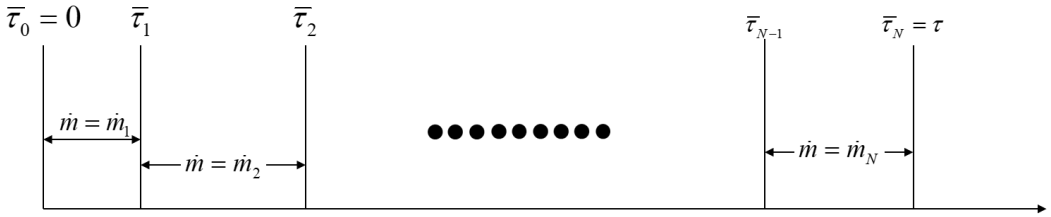

Figure 2. Breakdown of Operation Sequence by Time Intervals.

2.4 Thermal and Electric Power Estimation

For the purposes of power estimation due to the enthalpy gain in the fracture network alone, the following the temperature change from the fracture network exit to the surface through the riser will be ignored. The temperature gain down the wellbore will be assumed to be 15 ºC based on a conservative analysis of wellbore heat transfer.

Once the temperatures have been evaluated at a certain time instant corresponding to an assigned flowrate, the thermal power is estimated as

$$\dot{P}_{\mathrm{MWt}}(t) = \dot{m} c_{\mathrm{p}} \left[T_{\mathrm{exit}}(L,t) - T_{\mathrm{in}} \right] = \dot{m} c_{\mathrm{p}} \left(T_{\infty} - T_{\mathrm{in}} \right) \theta_{\mathrm{f}}(1,\tau) \tag{27}$$

where $\theta_{\mathrm{f}}(1,\tau)$ is obtained from the solution of Eq.(24). Electric power is then estimated in terms of the Carnot and thermal-to-electric conversion efficiencies as

$$\dot{P}_{\mathrm{MWe}}(t) = \eta_{\mathrm{Carnot}} \eta_{\mathrm{Conv}} \dot{P}_{\mathrm{MWt}}(t) - \dot{P}_{\mathrm{pump}}\left(\dot{m}, T_{\mathrm{exit}}\right) \tag{28}$$

where $\dot{P}_{\mathrm{pump}}$ is the (parasitic) power required to sustain the mass flow rate and the temperature dependence is responsible for the buoyancy effect in the riser wherein it is actually possible to operate without any pump power during the initial operation of the well system. The estimation of parasitic power is described in Appendix B.

2.5 Energy Management Algorithm

Assuming a certain target plateau electric power $\dot{P}_{\mathrm{Target}}$, and given resource and inlet temperatures and formation properties, the following algorithm is used to determine the mass flow rate to maintain the generated electric power at the target value over an operating time window:

1. Estimate the thermophysical properties from the average of the inlet and resource temperatures and hydrostatic pressure, and the capacity ratio Ψ from Eq. (19)
2. Set the Duhamel integrals corresponding to each Fourier mode to zero.
3. Divided the operating time window into several equally spaced intervals.
4. Initialise the time to zero
5. Guess a mass flow rate $\dot{m}$ and begin the following iterative loop
    a. Evaluate the velocity from Eq. (2)
    b. Evaluate the Modified Peclet number Ω from Eq. (18)
    c. Solve the dimensionless Energy Equation i.e., Eqs. (24) and obtain the temperature exiting the fracture $\theta_{\mathrm{f}}(1,\tau)$.
    d. Evaluate the Thermal Power from Eq. (27)
    e. Obtain the Electric Power estimate from Eq. (28)
    f. If the power is not equal to the target power, adjust the mass flow rate in accordance with a root-seeking procedure and repeat steps 5a—5e, otherwise proceed to Step 6
6. Update the Duhamel convolution integrals with Eq. (21)
7. Advance to the next time sub-interval using the temperature at the end of the previous sub-interval as the initial condition
8. Repeat Steps 5—7 until the end of the operating time window.

Some illustrative examples using the above algorithm are presented in what follows.

3. EXAMPLES AND DISCUSSION

3.1 Base Case Definition and Performance

The parameters corresponding to what will be designated the Base case are listed in the left panel Table 1. A resource at 5000 m TVD is assumed to have a temperature of 400 °C which is not unreasonable in terms of the temperature gradient of ~75 °C/km. It is assumed that 150 fractures are generated each with a height of 50 m and a thickness of 2 mm which are consistent with typical planar fracture geometries.

The fracture-to-fracture spacing of 10 m calls for a horizontal length of 1.5 km in the horizontal sections of the injector and riser wells which are spaced 100 m apart. This spacing is believed to be what is currently achievable in practice, although efforts to substantially enhance this spacing are underway, and these cases will be examined as sensitivities.

The thermal to electric power conversion efficiency is strictly speaking a function of exit temperature, but since this is a function of the surface equipment and not knowable a priori, a fixed value of 40% is assumed as a conservative estimate. The formation thermophysical properties are consistent with typical hot rock formations on the US West Coast, which is a rich area for tapping the potential of geothermal power.

The right panel of Table 1 lists the parameters independent of the mass flow rate that are used to estimate the dimensionless governing parameters Ψ and Ω that hold throughout the operating time window.

Table 1: Fracture Metrics and Operating Parameters for the Base Case.

Field Data		**Reference Conditions**	
Resource TVD (m)	5000	Temperature (°C)	225
Resource Temperature (°C)	400	Hydrostatic Pressure (MPa)	49.05
Fracture Dimensions		**Fluid Thermophysical Properties**	
# Fractures	**150**	Density (kg/m^3)	870
Length (m)	**100**	Specific Heat (J/kg-K)	4,367
Height (m)	**50**	Thermal Conductivity (W/m-K)	0.682
Thickness (mm)	3	Dynamic Viscosity (Pa-s)	1.30E-04
Frac-to-Frac Spacing (m)	**10.0**	Prandtl Number	0.833
Operating Parameters		**Fracture Geometrical Parameters**	
Inlet Temperature (°C)	50	Fracture Thickness (m)	0.003
W/B Temperature Gain (°C)	15	Fracture Flow Area (m^2)	7.50E-02
Working Fluid	WATER	Aspect Ratio	3.33E+04
Conversion Efficiency	40%	**Thermal Diffusivity (m^2/s)**	
Formation Properties		Fluid	1.79E-07
Thermal Conductivity (W/m-K)	2.0	Formation	6.17E-07
Specific Heat (J/kg-K)	1200	**Dimensionless Parameters**	
Density (kg/m^3)	2700	Ψ	**1.705**
		W	**3,333**

If a 10 MWe target is selected as the performance objective, Figure 3 shows that this target can be met over the entire period of a 5 year time window with the Base Case parameters. Due to the substantial buoyancy effect, the parasitic power see in the top panel of the figure is largely negligible ranging from 90 kW during the first few years and then starting to ramp up quite substantially to just under 1 MW by the end of the 5 year window in accordance with the higher mass flow rate (middle panel) required to offset the thermal decline evidenced in the exit temperature plot (the lower panel of Figure 3). Based on the steepness of the mass flow rate increase toward the end of the window, it can be surmised that production for any substantially longer period is not feasible, and this has to be noted in the context of energy planning and management. What is noteworthy is that the even towards the end of the operating window of 5 years, the exit temperature is above 300 °C which will prove very useful in the context of conversion efficiency, and in practice may actually render the flat 40% value assumed in Table 1 even more conservative than was anticipated.

3.1 Parametric Sensitivities

The effects of halving and doubling the fracture height are shown in Figure 4. All the other parameters are maintained at their Base Case values. An increase in the fracture height reduces the parameter Ω as evidenced by Eq. (18). This increase in flow area reduces the velocity and hence results in larger residence time in the fractures as the fluid crosses from the injector to the riser. The converse is true when the fracture height is reduced. .In the case of a 100 m fracture height, it is seen that 15 Mwe can be generated for just under 7 years while with a 25 m fracture height, the steeper drop off in exit temperature temperature due to a higher flow velocity results in unsustainably high required flowrates that limit 5 MWe to a little over 6 years.

While the current state of the art appears to limit fractures of length no greater than 100 m, efforts are underway to increase this to at least 250 m, .if not the 1000 m × 1000 m network that Gringarten (1967) had hypothesised in the illustrative example in his paper. The 5 year power generation is almost doubled in a length increase from 100 m to 250 m as seen in the curve corresponding to a 50 m fracture height in Figure 5. As the fracture height increases, the longer residence times result in higher exit temperatures upstream on the inlet to the riser, and therefore the length effect is seen to be less pronounced at a fracture height of 100 m than at 50 m.

The effect of fracture-to-fracture spacing is shown in Figure 6. Beyond a certain spacing distance, the cold front from the fractures propagating laterally outward have not yet reached the centerline symmetry plane in the 5 year time window considered in the plot. This explains the plateaus in both the 100 m and 250 m lengths considered. In all cases the fracture height is maintained at its base case value of 50 m. With this fracture height, a sustained 20 MWe power over 5 years is seen to be elusive. The reason for this becomes evident in

Figure 7 which shows that even at very early times and with an exit temperature equal to the resource temperature, the mass flow rate required results in a parasitic power of nearly 3 MWe that unlike that corresponding to the 10 MWe case of Figure 3 is not insignificant. As the temperature drops off with time the further increase in the required mass flow rate results in a parasitic power that is nearly half the net generated power close to the drop-off point at which the power target of 20 MWe can no longer be sustained. This occurs at just over 4 years.

As the resource temperature drops down to the subcritical regime (< 375 °C), Figure 8 not surprisingly shows a significant decline in the power generation capability with a power target of 10 MWe. The mass flowrate increase due to the exit temperature drop may in fact exceed the pumping power capacity at the surface, so that the actual drop off might be a bit earlier that those indicated in the figure.

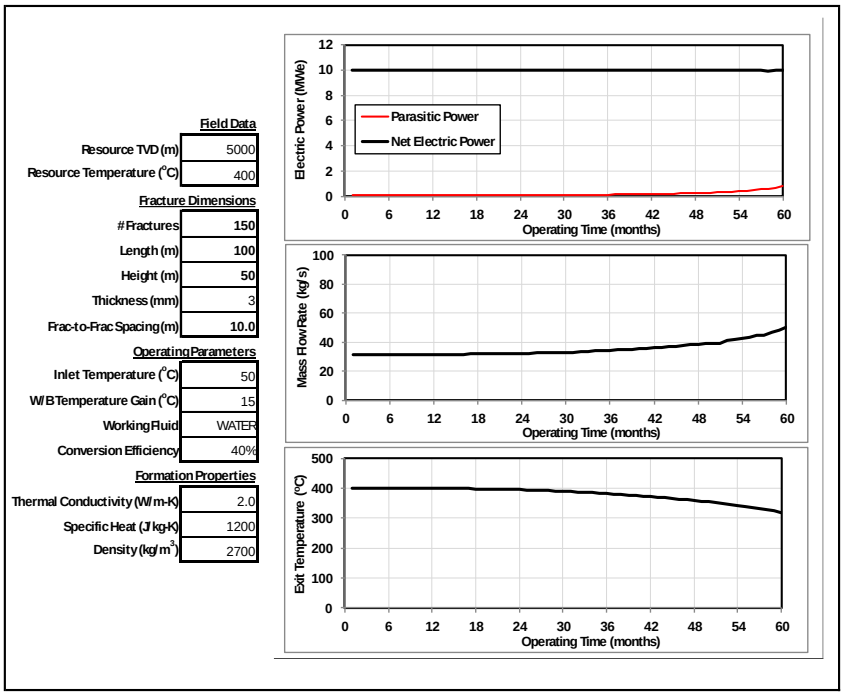

Figure 3. Sustained 10 MWe Production with the Base Case Metrics.

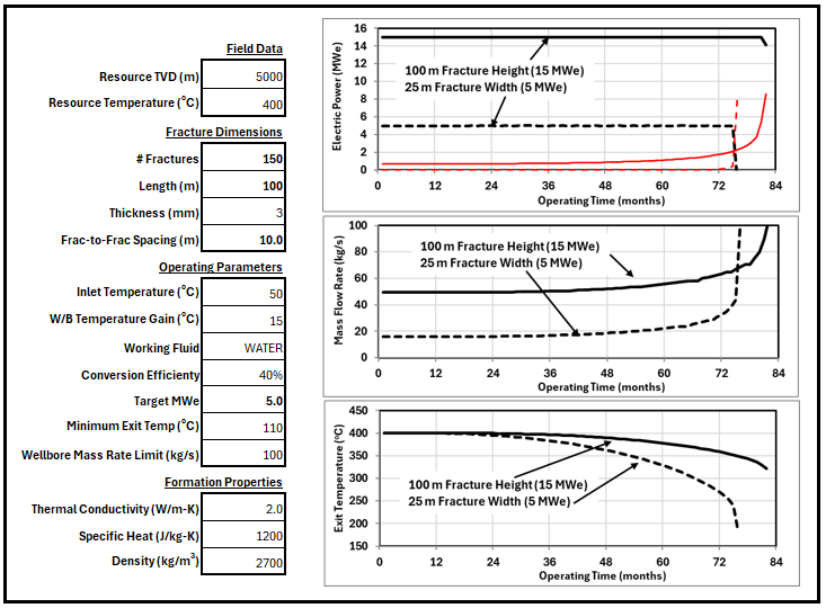

Figure 4. Effect of Fracture Height on System Performance.

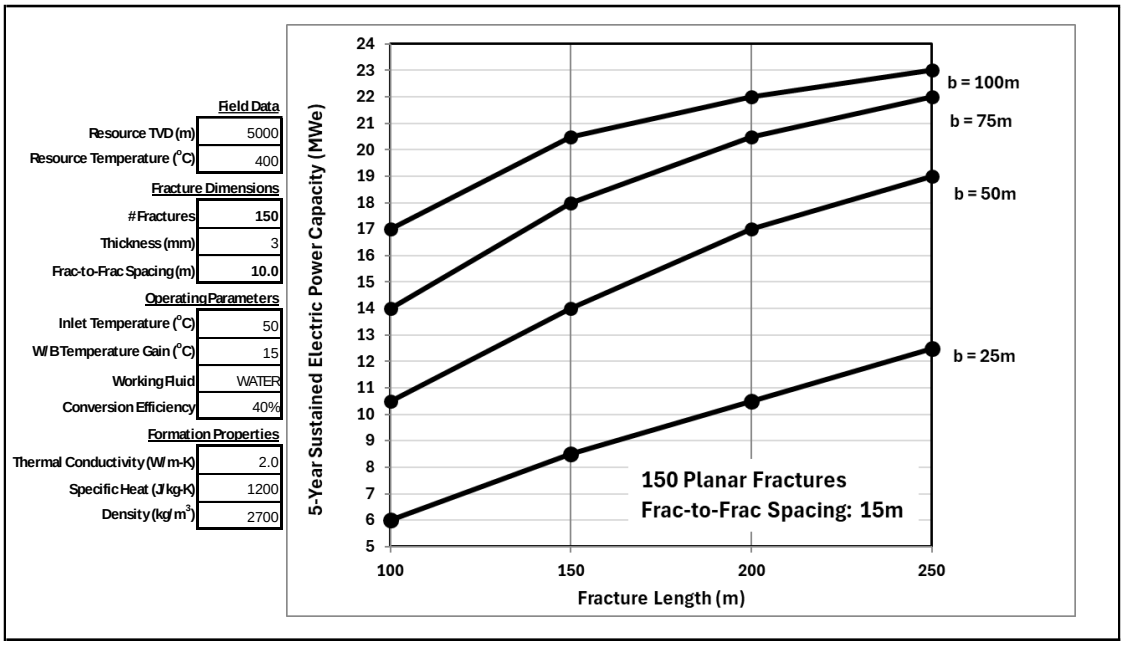

Figure 5. Maximum 5 year Sustained Power Generation as a function of Fracture Geometry.

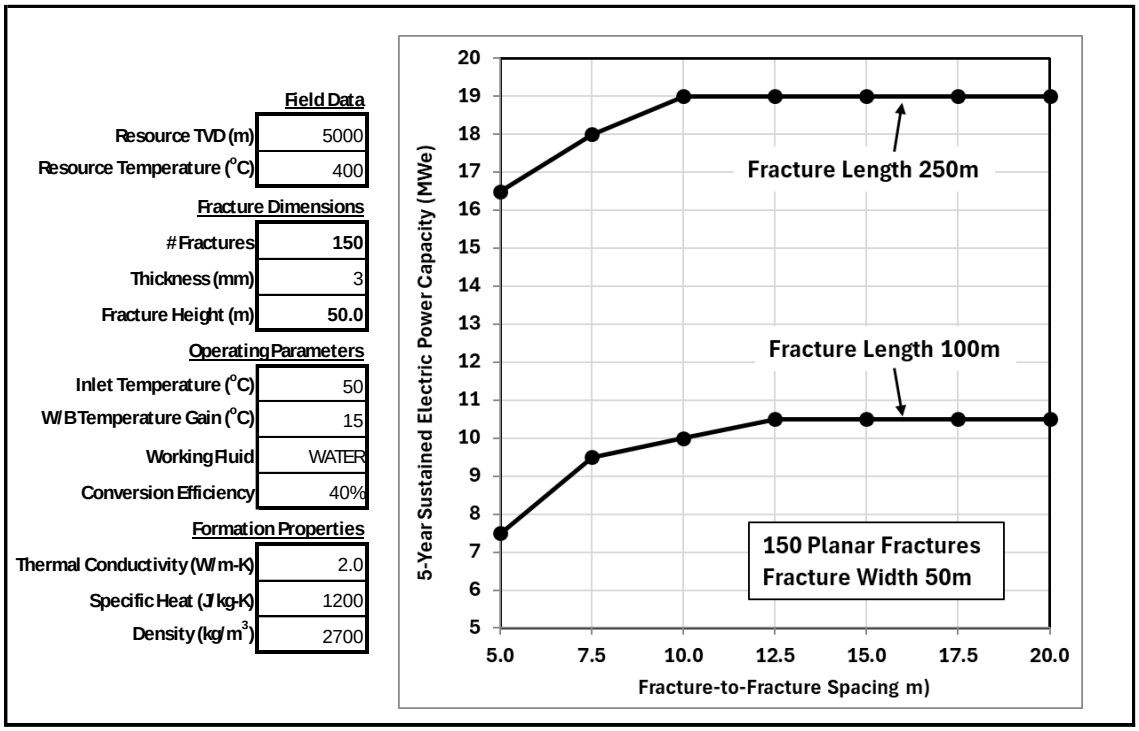

Figure 6. Maximum 5 year Sustained Power Generation as a function of Fracture-to-Fracture Spacing.

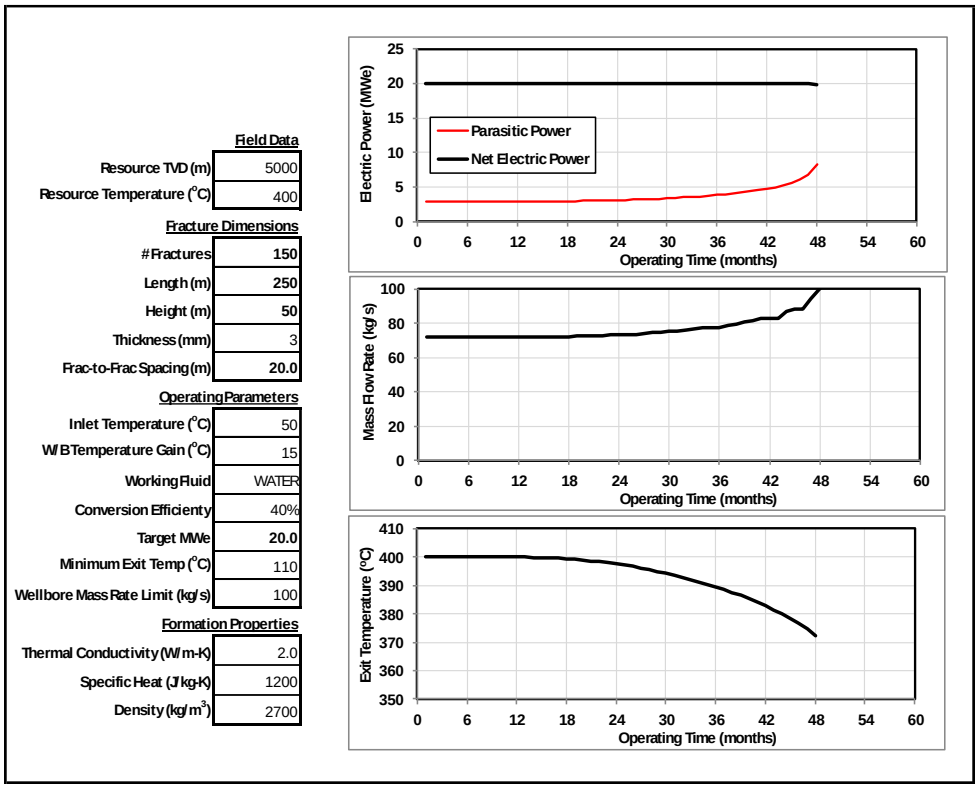

Figure 7. Effect of Higher Parasitic Power in response to a 20 MWE Target.

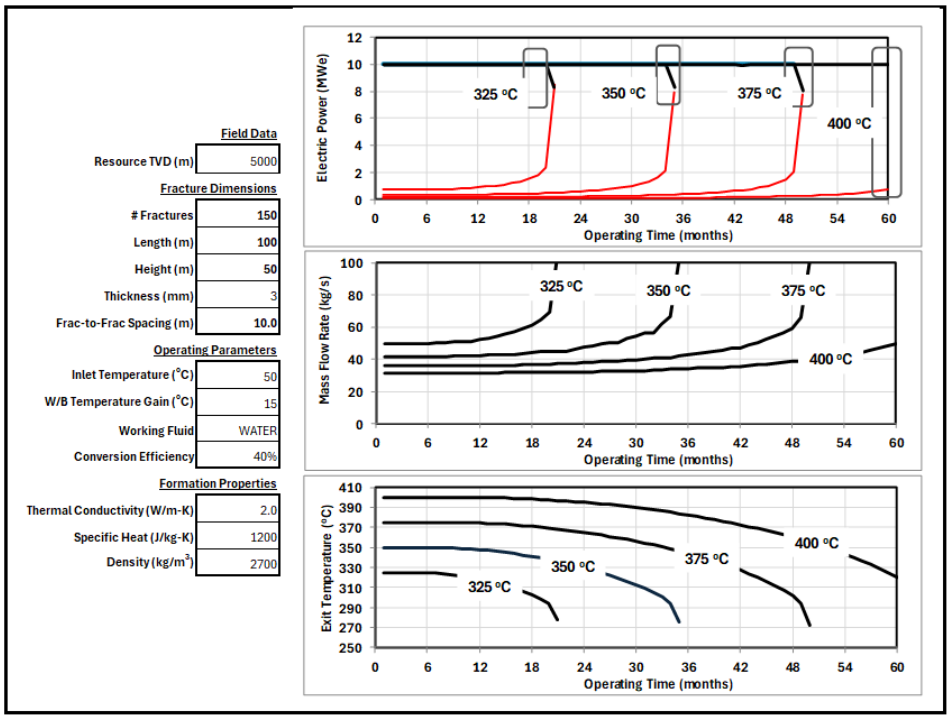

Figure 8. Effect of Resource Temperature on Power Generation.

The comprehensive performance summary in summary in Table 2 indicates that 5 MWe can be sustained for a 10 year period with a number of combinations of fracture dimensions and spacing. The number of options dwindle however as the target power increases, and in fact 20 MWe can only be sustained for a 10 year period with a fracture length of 250 m (not achievable with current technology) and a fracture height of 100 m (the upper limit of what may be achievable in practice over a length of 250 m).

It is noteworthy that the effect of fracture spacing is significant only at a power target of 5 MWe. This is because at the much higher mass flow rates demanded by higher power targets, the cold front from adjacent fractures tend to coalesce at the symmetry plane between fractures. There is a moderate effect of fracture spacing at a length of 250 m and higher power targets, due to the delayed coalescing of the cold fronts at the exit of the fractures into the riser well.

Table 2: Performance Summary over a range of Fracture Geometry Parameters, Fracture Spacing, and Target Power – Resource Temperature 400 ºC; 150 Fractures of Thickness 3 mm.

Main Body of Table is Time (Months) of Sustained Production at Target Power Level

Power Target: 5 MWe						
	Fac-to-Frac Half-Spacing = 10 m			Fac-to-Frac Half-Spacing = 15 m		
	L = 100m	L = 175m	L = 250m	L = 100m	L = 175m	L = 250m
b = 25m	75	160	250	90	210	345
b = 50m	190	375	565	255	525	600
b = 100m	440	>600	>600	>600	>600	>600
Power Target: 10 MWe						
	Fac-to-Frac Half-Spacing = 10 m			Fac-to-Frac Half-Spacing = 15 m		
	L = 100m	L = 175m	L = 250m	L = 100m	L = 175m	L = 250m
b = 25m	19	50	90	15	55	105
b = 50m	65	145	230	70	185	305
b = 100m	170	345	525	225	475	>600
Power Target: 15 MWe						
	Fac-to-Frac Half-Spacing = 10 m			Fac-to-Frac Half-Spacing = 15 m		
	L = 100m	L = 175m	L = 250m	L = 100m	L = 175m	L = 250m
b = 25m	5	15	35	5	15	35
b = 50m	20	65	110	20	70	135
b = 100m	80	180	285	90	225	375
Power Target: 20 MWe						
	Fac-to-Frac Half-Spacing = 10 m			Fac-to-Frac Half-Spacing = 15 m		
	L = 100m	L = 175m	L = 250m	L = 100m	L = 175m	L = 250m
b = 25m	0	5	10	0	5	10
b = 50m	5	25	50	5	25	50
b = 100m	30	85	150	30	95	175

Legend:

Red: **< 5 years**

Green **>10 years**

CONCLUSIONS

A fully transient analysis coupling the transport equation in the fracture to diffusion in the adjacent formation via a series of Duhamel Convolution integrals has been performed. The results indicate that for a given resource temperature, the fracture length and height are key parameters in achieving electric power capacities of 10 MW or greater for at least a 5 year period. The coalescing of thermal fronts can be mitigated by increasing the spacing between fractures. However past a certain threshold, this effect diminishes. The buoyancy effect eliminates the requirement for pumping (parasitic) power during the early years of power generation. However with inevitable thermal decline, the need for higher mass flow rates o offset the lower arrival temperatures calls for parasitic power that could at the of the time window be as much as 50% of the net power generated.

This work considers a well pair, primarily to illustrate the theoretical and semi-analytical framework and algorithm used to estimate constant power that can be achieved in an EGS project. The methods presented here can be extended to a field-wide analysis, thus informing field development strategies that maximize the magnitude and duration of constant power output, in the face of thermal decline. Such an analysis is beyond the scope of the current work. The practical implementation of the results demonstrated here would involve the creation of several well pairs or even triplets and well patterns considering that the fractures tend to propagate bilaterally. In this

context a proper mass flow rate schedule with well-by-well variations, and shut-in sequence to enable thermal recovery. could easily constitute a 100 MW power plant.

APPENDIX A: SOLUTION OF THE GOVERNING EQUATIONS

A.1 Transient Diffusion in the Formation

The solution of Eqs. (14)--(17) by Separation-of-Variables and the use of Duhamel's Principle is

$$\theta_{\mathrm{g}}(\eta,\tau)=\int_0^{\tau}\frac{\partial\bar{\theta}_{\mathrm{g}}}{\partial\tau}(\eta,\tau-\beta)\theta_{\mathrm{f}}(\beta)\mathrm{d}\beta \tag{A.1}$$

where the solution of the auxiliary problem is

$$\bar{\theta}_{\mathrm{g}}=1-\sum_{k=0}^{\infty}C_k e^{-\lambda_k^2\tau}\sin\lambda_k\eta \tag{A.2}$$

in which the eigenvalues and Fourier coefficients are

$$\lambda_k=\frac{1}{W}(2k+1)\frac{\pi}{2} \tag{A.3}$$

and

$$C_k=\frac{4}{(2k+1)\pi} \tag{A.4}$$

The interface flux appearing in the energy equation for flow in the fracture, i.e., Eq. (11) is

$$\left.\frac{\partial\theta_{\mathrm{g}}}{\partial\eta}(\tau)\right|_{\eta=0}=-\frac{2}{W}\sum_{k=0}^{\infty}D_k(\tau) \tag{A.5}$$

where the Duhamel Convolution Integral is

$$D_k(\tau)=\int_0^{\tau}e^{-\lambda_k^2(\tau-\beta)}\frac{\partial\theta_{\mathrm{f}}}{\partial\beta}\mathrm{d}\beta \tag{A.6}$$

which is in terms solely of the local fracture temperature. The interval 0 to τ can be divided into several subintervals such that the convolution integral in Eq. (A.6) can be split according to (see Chandrasekhar, 2019 for details)

$$D_k(\bar{\tau}_N)=\int_0^{\bar{\tau}_{N-1}}e^{-\lambda_k^2(\tau-\beta)}\frac{\partial\theta_{\mathrm{f}}}{\partial\beta}\mathrm{d}\beta+\int_{\bar{\tau}_{N-1}}^{\bar{\tau}_N}e^{-\lambda_k^2(\tau-\beta)}\frac{\partial\theta_{\mathrm{f}}}{\partial\beta}\mathrm{d}\beta \tag{A.7}$$

which with some algebraic manipulation is

$$D_k(\bar{\tau}_N)=e^{-\lambda_k^2\tilde{\tau}}D_k\left(\bar{\tau}^{(n-1)}\right)+\int_0^{\bar{\tau}_N-\bar{\tau}_{N-1}}e^{-\lambda_k^2(\tilde{\tau}-\beta)}\frac{\partial\phi_{\mathrm{f}}}{\partial\beta}\mathrm{d}\beta \tag{A.8}$$

where in the initial condition,

$$D_k(0)=0 \tag{A.9}$$

A.2 Laplace Transformation of the Transport Equation

Invoking the Convolution Theorem and skipping the details of algebraic minutiae, the partial differential equation of Eq. (24) can be Laplace-transformed to the ordinary differential equation in the frequency domain

$$\frac{\mathrm{d}\Phi_{\mathrm{f}}}{\mathrm{d}\xi}=-\left[\frac{s}{\Omega^{(n)}}\left(1+2\frac{\Psi}{W}G\right)\right]\Phi_{\mathrm{f}}+\frac{1}{\Omega^{(n)}}\left(\phi_{\mathrm{f}}(\xi,0)-2\frac{\Psi}{W}H\right) \tag{A.10}$$

where

$$G = \sum_{k=0}^{\infty} \frac{1}{s+\lambda_k^2}, \qquad H = \sum_{k=0}^{\infty} \left[\frac{D_k\left(\bar{\tau}^{(n-1)}\right) - \phi_f\left(\xi,0\right)}{s+\lambda_k^2} \right] \tag{A.11}$$

subject to the boundary condition

$$\Phi_f\left(1,s\right) = \frac{1}{s} \tag{A.12}$$

Except at $\tau = 0$ where $\phi_f\left(\xi,0\right)$, an analytical solution of Eq. (A.10) and the instantaneous local initial condition has to be linearised. Accordingly inversion with the Residue Theorem would involve a book-keeping ordeal that is not worth the computational expense, and inversion back to physical space with a Gaver-Stehfest function sampling approach is more efficient.

APPENDIX B: PARASITIC POWER

Subject to the constraint of a specified riser exit pressure at Station 5 in Figure 9,, the pressure at station 1 (the injector inlet) has to be determined iteratively for a given mass flow rate, rom the sequence of equations for Stations 2 –5. For a given well geometry, number of planar fractures, and fracture spacing, this can be computed for a range of mass flow rates and the parasitic power can be determined by interpolation from a lookup table. The parasitic power required is

$$\dot{P}_{\text{pump}}\left(\dot{m}, T_{\text{exit}}\right) = \text{Max}\left[2\frac{\dot{m}}{\rho_1 + \rho_5}\left(P_1 - P_5\right), 0 \right] \tag{B.1}$$

for a given well geometry and resource depth, and at flow rates less than a certain threshold, the lower densities in the riser generate a buoyance effect that entirely obviates the need for any pumping power. since $P_5 > P_1$, and in fact at very low flow rates, P_1 can in fact be atmospheric pressure. For cases where P_1 is greater than atmospheric pressure but still less than the exit pressure, it is assumed that the pressure drop of the working fluid across the surface equipment still ensures the required injector inlet pressure without the need for any pump power.

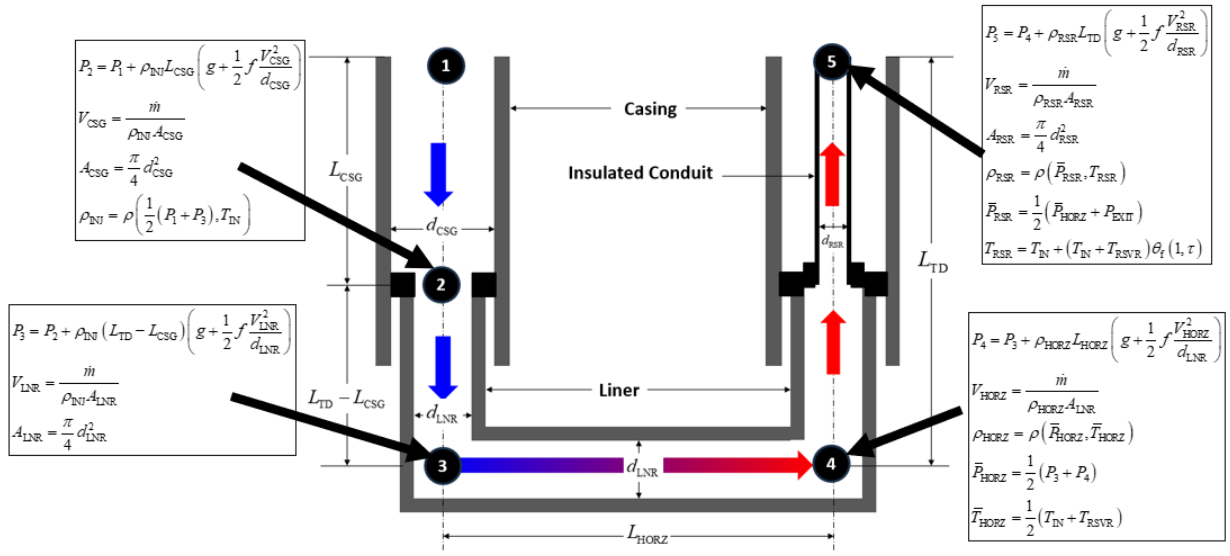

Figure 9. Parasitic Power Estimation Methodology.

For the parameters listed in the left panel of Figure 10, the required pump power and pump inlet pressure show that the buoyancy effect eliminates the need for any pumping power up to 40 kg/s. However as the required flowrate exceeds 80 kg/s, the pump power exceeds the working capacity of most surface equipment.

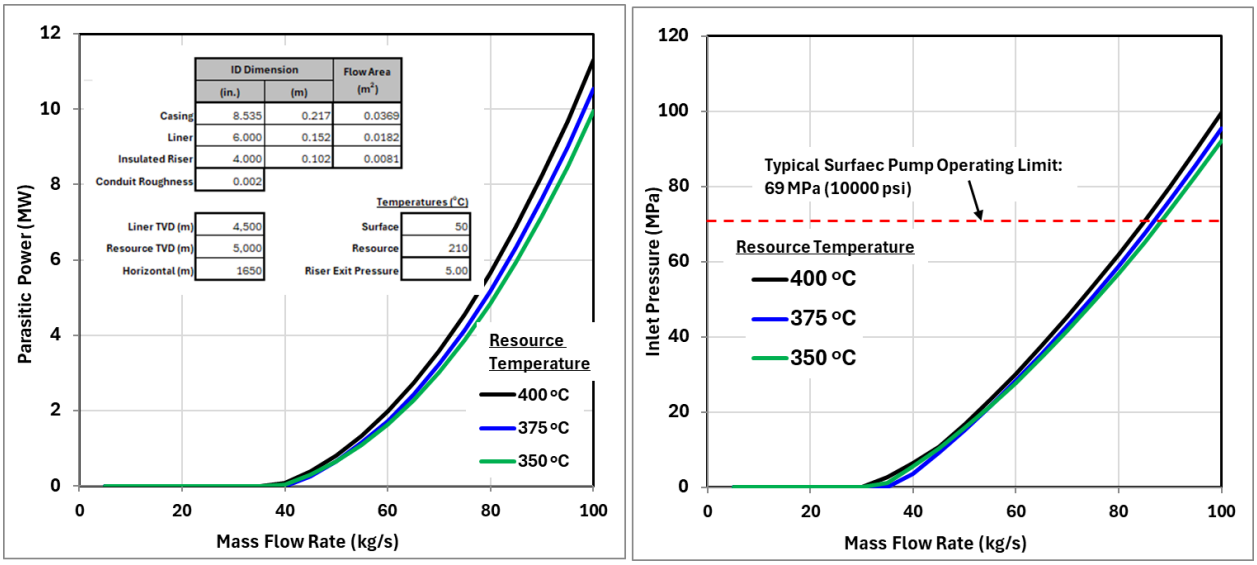

Figure 10. Parasitic Power dependency on Mass Flow Rate and Resource Temperature.

NOMENCLATURE

b	m	Fracture Height
c_p	J/kg-K	Specific Heat at constant pressure
k	W/m-K	Thermal Conductivity
$\dot{m}$	Kg/s	Mass Flow Rate
t	sec	Time
T	°C	Temperature
V	m/s	Fluid Velocity
w	mm	Fracture Thickness
x	m	Lateral coordinate Perpendicular to Fracture
x_C	m	Half-Spacing between fractures
z	m	Streamwise coordinate along Fracture

Subscripts

f	Fluid in Fracture
g	Formation
∞	Undisturbed Geothermal

REFERENCES

Chandrasekhar, S., Suryanarayana, P.V., Sathuvalli, U.B., and Asher, G.: Scaling and Thermal Penetration Depth in Enhanced Geothermal Energy Production, GRC Transactions Vol. 48, Waikiloa, HI, (2024).

Suryanarayana, P.V. and Chandrasekhar, S.: Optimizing Mass Flow Rate in Enhanced and Advanced Geothermal Systems using Scaling Parameters, 50th Workshop on Geothermal Reservoir Engineering, Stanford University, Stanford, California, February 10-12, (2025).

R. Allis, and J. N. Moore, Geothermal Characteristics of the Roosevelt Hot Springs System and Adjacent FORGE EGS Site, Milford, Utah, Utah Geological Survey (2019).

Beckers, K.F., Rangel-Jurado, N., Chandrasekar, H., Hawkins, A.J., Fulton, P.M., and Tester, J.W., "Techno-Economic Performance of Closed-Loop Geothermal Systems for Heat Production and Electricity Generation", Geothermics, v. 100, p. 102318 (2022)

Brown, D., Duchane, D., Heiken, G., and Hriscu, V., Mining the Earth's Heat: Hot Dry Rock Geothermal Energy, Springer (2012)

H. J. Ramey, Jr., “Wellbore Heat Transmission”, SPE Paper 96, March (1962).

US Department of Energy, “Pathways to Commercial Liftoff: Next-Generation Geothermal Power”, Public Report, March (2024)

Chandrasekhar S. Revisiting the Classical Problem of Transient Temperature Prediction in Complex Deepwater Wellbores with a New Semi-Analytical Approach", SPE/IADC Paper 199653. Galveston, TX , March 3--5, (2020).

Gringarten, A. C., Witherspoon, P. A., and Ohnishi, Y., “Theory of Heat Extraction from Fractured Hot Dry Rock”, Journal of Geophysical Research, Vol 80, N0. 8, (1975).

Holmes, M., Toews, M, Jenkins, J., and Sepulveda, N., Multilateral Closed-Loop Geothermal Systems as a Zero Emission Load-Following Resource, GRC Transactions, Vol. 45 (2021).

Moncarz, P. D., and Suryanarayana, P. V., “Harvesting GeoHeat and the Impact of Enhancing Thermal Reach on Energy from Hot Dry Rock”, United States Military Academy Special Colloquium on Computational Engineering Mathematics, West Point, October 21-22 (2022)

Norbeck, J., Latimer, T., Gradl, C., Agarwal, S., Dadi, S., Eddy, E., Fercho, S., Lang, C., McConville, E., Titov, A., Voller, K., and Woitt, M., 2023, “A Review of Drilling and Stimulation of a Horizontal Geothermal Well System in North Central Nevada”, 48th Stanford Geothermal Workshop, February 6-8, (2023).